J Mater Sci (2008) 43:5809–5822
DOI 10.1007/s10853-008-2884-7

Sol–gel processing and UVA patterning of epoxy-based hybrid organic–inorganic thin films

S. Briche · D. Riassetto · C. Gastaldin · C. Lamarle · O. Dellea · D. Jamon · E. Pernot · M. Labeau · G. Ravel · M. Langlet

Received: 17 June 2008 / Accepted: 16 July 2008 / Published online: 31 July 2008

Abstract Sol–gel processed photosensitive hybrid organic–inorganic films, deposited from 2-(3,4-epoxycyclohexylethyltrimethoxysilane) (EETMOS), have been studied. EETMOS sols have been optimized with respect to several criteria that guarantee a good quality, photosensitivity, and reproducibility of derived films. Photo-sensitivity of EETMOS-based films has been assessed by UVA exposure experiments. Optimized films have been photo-patterned using a mercury lamp or a He–Cd laser source, both emitting in the UVA spectral range. Promising micronic size motives have been laser patterned. The quality of derived motives is discussed with respect to photopolymerization mechanisms and photo-patterning parameters.

Introduction

Since early 1990s, sol–gel processing of photopolymerizable hybrid organic–inorganic thin films has been extensively developed for applications in integrated optics, in order to fulfil increasing demands for miniaturized optical devices [1–15]. These films have been deposited from precursors that associate silicon alkoxyde groups, reactive to sol–gel reactions, with photosensitive organic groups. Resulting films combine the glass-like behaviour of a silica-based inorganic component (optical quality, enhanced thermal and chemical stability and so on) and photosensitivity of the organic component. This latter can polymerize under UV light in presence of a photo-initiator. It allows the direct fabrication of optical devices through lithographic procedure and subsequent wet-etching of the non-polymerized areas, yielding a negative resist-like pattern. Such a method greatly simplifies lithographic processes compared to multi-step and time consuming traditional procedures. In published works, the organic component of photosensitive sol–gel hybrid films is generally based on acrylate or methacrylate groups that react upon UV irradiation through a radical polymerization mechanism. Such compounds exhibit high photo-conversion rate under UV, but the radical polymerization can seriously be inhibited by atmospheric oxygen [16], which in turn reduces the photo-conversion yield, especially in thin films. Epoxyde compounds are another class of photosensitive materials that readily react under UV light through a cationic polymerization mechanism using adapted photo-initiator [16–19]. Triarylsulfonium salts have commonly been used as cationic photo-initiators to induce the photopolymerization of all-organic epoxy-based materials [16, 18]. Broadly speaking, these salts generate acid or cation intermediate species upon UV irradiation, which can open the epoxy ring of a vicinal monomer to form an oxiranium ion. This ion reacts then with a new epoxyde monomer, which initiates chain reactions and propagation of an organic polymer network constituted of polyether chains. Since this mechanism is insensitive to oxygen, epoxyde compounds appear as a

S. Briche · D. Riassetto · C. Gastaldin · E. Pernot · M. Labeau · M. Langlet (✉)
LMGP, Grenoble INP, Minatec BP 257, 38016 Grenoble Cedex 1, France
e-mail: michel.langlet@inpg.fr

C. Lamarle · O. Dellea
PF D2M/CEA LITEN, 18 Rue Benoît LAURAS, Bât. G, 42000 St. Etienne, France

D. Jamon
DIOM, Université Jean Monnet, 23 rue Paul Michelon, 42023 St. Etienne, France

G. Ravel
CEA LITEN, 17 rue des Martyrs, 38054 Grenoble Cedex 9, France

suitable alternative for acrylates or methacrylate ones. Surprisingly, very few photopolymerizable epoxy-based hybrid organic–inorganic films have been studied. Only some rare and recent articles mention their deposition for the fabrication of integrated optical devices. Cheng et al. [20] reported on the deposition of silicone-epoxyde hybrid films, using a siloxane crosslinker. The films were patterned through a nano-imprinting process followed by UV curing, showing the photopolymerization efficiency of epoxy groups immobilized in hybrid organic–inorganic films. However, as-deposited silicone-epoxy liquid films were observed to dewet and bead up when deposited on a silicon substrate. Such behaviour, which restrained the film deposition to polymeric substrates, occurred owing to surface tension effects that could not be counteracted by the formation of sufficiently strong chemical bonds in the film. Since, during the post-deposition liquid–solid transformation, the sol–gel process yields development of an inorganic network constituted of Si–O–Si polymeric chains, it provides a suitable alternative to prevent such dewetting effects by reinforcing strength of chemical bonds in the film. Accordingly, Brusatin et al. [21] succeeded in the deposition of silica-epoxyde hybrid films, using 3-glycidoxypropyltrimethoxysilane (GPTMS) as an epoxyde sol–gel precursor, and they studied the photopolymerization of their films in relation to the nature of cationic photo-initiators. These authors reported on the nanopatterning of such films using electron or X-ray radiation [22]. They also studied UV patterning of their epoxy-based films through a direct method without post-irradiation etching, which was based on a local, but limited, densification of the film in UV irradiated areas [23]. Recently, Jabbour et al. [24–26] studied the fabrication of good quality optical circuits through UV laser patterning and post-irradiation etching of sol–gel hybrid films deposited from 2-(3,4-epoxycyclohexylethyltrimethoxysilane) (EETMOS) as an epoxy precursor, showing the high photoconversion rate of EETMOS derived films.

Since the amount of published articles is extremely limited, the study of UV photopolymerizable epoxy-based sol–gel hybrid films remains a subject of interest, both from academic and applicative point of view. In this paper, we present new studies of photopolymerizable sol–gel films deposited from EETMOS. Objectives of this work are twofold. In a first part, we study optimization of the EETMOS sol with respect to the overall quality and photosensitivity of derived films. The sol–gel reactivity of an ideal sol intended to deposit photopolymerizable hybrid films should fulfil several criteria. On the one hand, the sol should be reactive enough in order to prevent detrimental film dewetting effects. It is known that sol–gel precursors containing photosensitive groups are poorly reactive to hydrolysis/polycondensation reactions, which inhibits the post-deposition gelation [27, 28]. This is due to steric hindrance of aliphatic chains that reduces chemical interactions between alkoxy groups reactive to sol–gel reactions. Specific formulations have thus to be set up to activate reactions in the sol. On the other hand, the sol–gel reactivity should not be too high in order to formulate stable sols, which will determine the in-time reproducibility of thin films using a same sol. Finally, the sol–gel reactivity should not induce a premature consumption of reactive epoxy groups in the sol, which would reduce the photosensitivity of deposited films. In their work, Jabbour et al. [25] controlled the reactivity of EETMOS-based sols through a two-step preparation process, using hydrochloric acid (HCl) in a first step and hydrofluoric acid in a subsequent step. Nuclear magnetic resonance studies showed that these acids acted as efficient catalysts of the hydrolysis/polycondensation sol–gel reactions. These authors also mentioned that their sol formulations partially yielded a premature consumption of epoxy groups [26], and they did not report on the in-time stability of so-obtained sols. In this paper, we have chosen to control our sol reactivity through the combination of (i) an acidic catalysis of the sol–gel reactions using HCl, (ii) a chemical activation of these reactions by adding in the sol a pure silicon alkoxyde (tetraethoxysilane, TEOS) co-reactant and (iii) a thermal activation of the reactions by heating the sols in oven at 60 °C. In a second part of this paper, we study the feasibility of photo-patterned devices from our hybrid films. Tests have first been performed through a traditional photolithographic process using a chromium mask under 365 nm wavelength irradiation. Nevertheless, in a context of R&D requiring rapid prototyping, such a process presents several limitations like the price or time spent for the design and fabrication of the masks. Moreover, photolithographic processes using a mask do not allow to pattern films with high aspect ratio. This is the reason why some of us are engaged in a national R&D project (MOSAHYC project) focused on a maskless laser imprinting method. Such a method appears to be very promising, since it can considerably reduce operation costs and simplicity of the lithographic process. The ultimate goal of the present work is, therefore, to study the feasibility of UV laser imprinting on EETMOS-based hybrid films. Previous studies devoted to laser photo-patterning of such films were performed using a frequency quadrupled Nd:YLF laser emitting in the UVB spectral range (262-nm wavelength) [24–26]. In this paper, photo-patterning has been studied using a laser emitting in the UVA range (325 nm). To the best of our knowledge, patterning of EETMOS-based hybrid films using UVA light has never been previously tested. Feasibility of laser photo-patterning of such films using UVA light would extend applications of these films to a larger range of laser sources including common sources such as He–Cd lasers. Thus, the overall issue

studied in this paper is to study the deposition of good quality EETMOS-based films and to assess their photosensitivity in the UVA range.

Experimental

EETMOS sol formulations

EETMOS and TEOS were purchased from Aldrich and STREM Chemicals, respectively. EETMOS was first partially hydrolyzed in deionized water acidified with HCl. The water to EETMOS molar ratio was fixed at 0.6 for an EETMOS concentration of 3.9 M and a pH of 0.7. Triarylsulfonium hexafluorophosphate (TFP, initially diluted at 50 wt% in propylene carbonate) purchased from Aldrich was used as a photo-initiator. This compound essentially absorbs in the UVB spectral range and exhibits a weakly intense absorption tail that overlaps the UVA range. The TFP solution was preliminary diluted in methanol and then added to the EETMOS sol. The TFP/EETMOS ratio was fixed at 1.5 wt%. In a separate flask, TEOS was prehydrolyzed in deionized water acidified with HCl. The water to TEOS molar ratio was fixed at 2.2 for a TEOS concentration of 3.8 M and a pH of 2. EETMOS and TEOS solutions were then mixed in various TEOS/EETMOS ratios. In this paper, sols and derived films will be labelled with respect to the TEOS/EETMOS molar ratio, e.g. S40 for a sol (or derived film) with a TEOS/EETMOS molar ratio of 40%. Deionized water was then added in the mixed sol to complete hydrolysis of EETMOS and TEOS. The water to [EETMOS–TEOS] molar ratio was fixed at 1.6. The final solution (EETMOS–TEOS concentration of 3.6 M) was then aged for various durations in oven preheated at 60 °C. It was finally diluted in absolute ethanol to fix EETMOS–TEOS concentrations ranging from 0.5 to 3.6 M.

Hybrid film deposition and processing

Hybrid thin films were deposited at room temperature by spin-coating on (100) silicon wafers or soda-lime glass plates. Small size substrates (3×3 cm^2) were routinely coated with 300 μL of sol using a Suss Microtec RC8 apparatus operated at 3,000 rpm. In some cases, film deposition was attempted with greater sol volumes up to 6 mL in order to deposit thicker films, and tests were also performed on 4-in. diameter silicon wafers in order to test the large scale thickness homogeneity of deposited films. These latter tests were performed using a Suss Microtec DELTA 80 RC spin-coater operated at 3,000 rpm. Prior to deposition, the substrates were cleaned with ethanol and dried with air spray. After liquid film deposition, the solvent rapidly evaporated and a xerogel film formed at ambient atmosphere through the hydrolysis/polycondensation sol–gel route. Xerogel films were then used as-deposited for characterization and/or exposition to UV sources. In some cases, films heat-treated in air at 80 °C for 10 min were also studied. Photo-patterning was first tested on the different films using a glass-supported chromium mask constituted of strips of various micronic width and spacing. These tests were performed using a mercury lamp, which essentially emitted at 365 nm (light power density of ca. 15 mW/cm^2). The experimental device was thermalized at around 40–45 °C. Preliminary tests showed that, at this temperature, thermally induced modifications of the film (polymerization of the organic component, sol–gel transformation of the inorganic component) were negligible. Laser photo-patterning tests were then performed using a commercial device (Dilase 750). This device is equipped with a He–Cd laser source emitting at 325 nm whose light power can be adjusted. A devoted optical arm enables to shape and focalize the laser beam on the sample to be patterned. The focalized laser beam has a circular symmetry and a constant diameter whose lowest value is of 4 μm. Moreover, the optical arm ensures a field depth >10 μm. Focalization of the laser beam is achieved through a lens mounted on a micrometric screw which allows a precise positioning in relation to the sample to be patterned. In next parts of this paper, position of the lens is defined with respect to an arbitrary zero value. The sample is dynamically irradiated by being translated under the laser beam using a computer-driven micro-displacement system. In this paper, the light power was fixed at its nominal value of 30 mW. The imprinting speed, i.e. displacement speed of the sample under the laser beam, was varied between 0.5 and 5 mm/s. Strips of 2-mm length were imprinted at 0.1 mm intervals using a constant speed and lens position. After each strip imprinting, the lens position was modified by 10 μm steps, in a -200 to $+200$ μm position range with respect to the zero position, in order to define best focalization conditions of the laser beam. After UV exposure, through a mask or using laser beam, films were washed by rapid aspersion with absolute ethanol in order to etch non-irradiated areas.

Film characterizations

UV/visible transmittance spectra of films deposited on glass were measured in the range of 200–1100 nm using a Jasco V-530 spectrophotometer. All other characterizations were performed on films deposited on silicon. Reactivity features of the different sols were studied through an analysis of infrared spectra of the derived films. Fourier transform infrared (FTIR) spectra were acquired in

transmission configuration in the 4,000–250 cm^{-1} spectral range using a Bio-Rad FTS-165 spectrometer. Spectra of 300 scans were recorded in room atmosphere under dry air sweeping with a resolution of 4 cm^{-1}. The spectra were analysed after subtraction of the bare silicon substrate spectrum. A same methodology was used to analyse the photo-induced features in films exposed for various durations to the UV lamp without mask. Refractive indices and thicknesses of the films were routinely measured by monochromatic ellipsometry using a Gaertner L116B ellipsometer operated at a 633 nm wavelength. More punctually, spectroscopic ellipsometry measurements were also performed using a Jobin Yvon—Horiba Uvisel ellipsometer. Quality and width of photo-patterned strips were assessed from optical observations using a Leica DMLM or a Nikon Eclipse ME600 microscope. Profiles of the photo-patterned strips were analysed by field emission gun scanning electron microscopy (FEG-SEM), after cleavage of the Si wafer, using a HITACHI S-4500 microscope operated at 5 kV, and atomic force microscopy (AFM) using a Digital Instrument Nanoscope microscope in contact mode. Heights of the strips were evaluated by AFM analysis and by profilometry measurements using a Dektak 3ST apparatus.

Results and discussion

Sol reactivity features

In this section, we analyse how the sol formulation influences reactivity features, and how these features impact the film quality. The concentration of TEOS and EETMOS in the sols was observed to moderately influence reactivity features, i.e. the sol reactivity gradually increased when increasing the precursor concentration, and these effects had minor consequences on the film quality. Thus, in this section, concentration effects are not studied in details and we focus on the effects of TEOS addition and sol ageing at 60 °C. Figures 1–3 show typical FTIR spectra of films deposited from sols with various TEOS content, aged or not at 60 °C. Since films deposited from the various solutions could present thickness differences, IR spectra were normalized with respect to a band, located at 2,930 cm^{-1} (not shown here), and assigned to saturated CH_2 aliphatic groups from EETMOS [26]. This band also corresponds to a very minor band of ethoxy groups from TEOS, which can be neglected in this normalization (see below). CH_2 aliphatic groups from EETMOS are assumed to be non-reactive to organic polymerization and sol–gel reactions. This normalization allows, therefore, a reliable comparison between bands intensities of the different reactive species present in films of various thicknesses [26]. Main reactivity

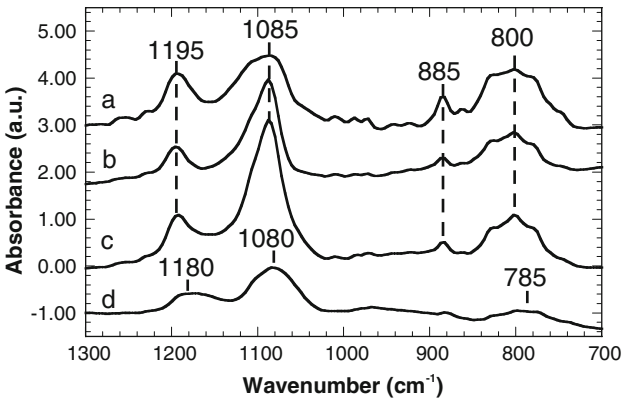

Fig. 1 IR spectra of films deposited from pure EETMOS sol (a), non-aged S0 sol (b) non-aged S40 sol (c) and S40–S0 differential spectrum (d). The EETMOS–TEOS concentration was fixed at 3.6 M

features were observed in the 1,300–700 cm^{-1} IR range. Spectra corresponding to non-aged sols are compared to that of pure EETMOS in Fig. 1. The EETMOS spectrum (Fig. 1a) essentially exhibits bands corresponding to methoxy groups at around 1,195, 1,085 and 800 cm^{-1}, which are commonly observed in the spectra of xerogels prepared from tetramethoxysilane [29]. A band located at 885 cm^{-1} is assigned to epoxy rings from EETMOS [17]. Other minor IR features are out of the topics of this paper. Spectra of films deposited from non-aged S0 (Fig. 1b) and S40 sols (Fig. 1c) are quite similar to that of EETMOS, essentially showing methoxy bands. In these spectra, a decrease in relative intensity of the epoxy band can be appreciated when compared to the EETMOS spectrum. It is presumably related to partial consumption of epoxy cycles in our acidic sols in presence of water. It is well known that, under acidic conditions, epoxyde rings can be hydrolytically opened to form glycols [30–32]. These latter species are no longer reactive to photopolymerization, which means that their formation in the sol should be minimized when considering the deposition of photosensitive films. It has been reported that the action of mineral or organic acids in the ring opening reaction depends on the nature of the acid, and action of HCl is rather limited [32]. Compared to that of EETMOS, spectra of S0 and S40 films show a relative intensity increase of the 1,085 cm^{-1} band. It is attributed to the growth of the main vibration band of silica (TO3 mode at 1,080 cm^{-1}) [33], showing that silica chains develop during the post-deposition sol–gel transformation through hydrolysis/polycondensation of alkoxyde groups. Silica chain development is supported by the S40–S0 differential spectrum of Fig. 1d, which exhibits typical bands of silica at 1,180 (LO3 mode), 1,080 (TO3 mode) and 785 cm^{-1} (TO2 mode) [33]. In the spectrum of Fig. 1c, these bands are superimposed to methoxy bands. The differential spectrum of Fig. 1d suggests in turn that

adding TEOS to EETMOS increases the sol reactivity. However, S0 and S40 spectra do not show significant differences in the intensity of methoxy bands from EETMOS. In contrast, TEOS bands cannot be observed in the S40 spectrum, in particular a band located at around 950 cm^{-1}. This band is conjointly assigned to non-hydrolyzed ethoxy groups from TEOS and to silanol groups issued from hydrolysis of alkoxy groups [33]. Absence of this band in the spectrum of an S40 film indicates that TEOS has been fully consumed by hydrolysis/polycondensation reactions (which also supports that the TEOS component at 2,930 cm^{-1} can be neglected in our normalization). All these observations suggest that, in films deposited from non-aged TEOS-based sols, TEOS reacts with itself without producing an enhanced reactivity of EETMOS. Resulting S40 films are thus presumably constituted of silica shells dispersed in EETMOS-rich regions, rather than a continuous inorganic silica network issued from the hetero-condensation of ethoxy groups from TEOS with methoxy groups from EETMOS. Accordingly, corresponding films were observed to severely dewet and partially denude the silicon substrate. As mentioned in the section "Introduction", insufficient sol reactivity yields weak strength of chemical bonds in the films, which are not able to counteract surface tension effects, leading thus to dewetting defects. Since they are much more reactive than TEOS, alkoxydes of transition metals, such as titanium or zirconium alkoxydes, are traditionally used to enhance the reactivity of sols derived from acrylate or methacrylates hybrid precursors [1–15]. However, it is known that these alkoxydes activate opening of the epoxy cycles in the sol, yielding polymerization of polyethylene oxide chains [8, 30, 32]. Since these chains are no longer sensitive to UV photopolymerization, their formation should be prevented as well in the sol. This is the reason why we chosen to co-react EETMOS with TEOS, as polymerization in polyethylene oxide chains cannot be induced by silicon alkoxydes [30]. Accordingly, intensity of the epoxy band at 885 cm^{-1} does not differ between S0 and S40 spectra of Fig. 1. However, this figure also indicates that reactivity of sols processed at room temperature remains quite limited.

Figure 2 shows the spectra of S40 films issued from sols aged at 60 °C for various durations. These spectra illustrate a continuous decrease in intensity of methoxy bands during sol aging at 60 °C, it showing a thermal activation of the methoxy consumption through sol–gel reactions. These reactions yield the development of silica chains whose IR signature is superimposed to remaining methoxy bands, as already shown in Fig. 1. In the same time, the epoxy band at 885 cm^{-1} is also observed to decrease over aging, which suggests that heating the sols at 60 °C promotes as well a thermal activation of the undesired hydrolytic opening of epoxy rings. This intensity decrease is associated to a

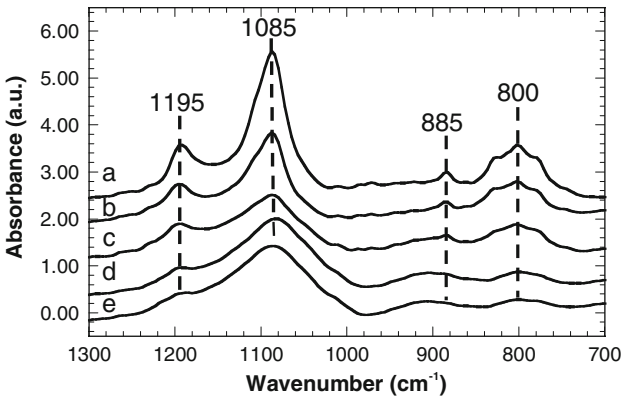

Fig. 2 IR spectra of S40 films deposited from a non-aged sol (a) and from a sol aged at 60 °C for 16 h (b), 22 h (c), 36 h (d) and 48 h (e). The EETMOS–TEOS concentration was fixed at 1 M

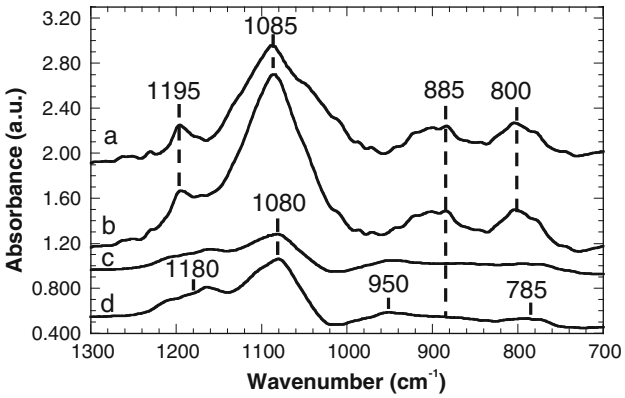

Fig. 3 IR spectra of films deposited from S0 (a) and S40 sols (b) aged at 60 °C for 36 h, and differential spectra S20–S0 (c) and S40–S0 (d) for the same sols. The EETMOS–TEOS concentration was fixed at 3.6 M

broadening of the 885 cm^{-1} band towards greater wavenumbers, which might be assigned to the formation of glycols arising from epoxy ring opening [26]. Figure 3 shows the spectra of S0, S20 and S40 films deposited from sols aged at 60 °C for 36 h. The overall spectra (Fig. 3a, and b) are dominated by bands of residual epoxy and methoxy groups. However, S20–S0 (Fig. 3c) and S40–S0 (Fig. 3d) differential spectra clearly show that increasing the TEOS content in the sol promotes an increase in intensity of the bands assigned to silica chains (1,180, 1,080 and 785 cm^{-1}), which are observed to grow together with a weak band at 950 cm^{-1} assigned to chain-end silanol groups. Contrary to what occurs in sols aged at room temperature, methoxy consumption illustrated in Fig. 2 suggests that, in sols aged at 60 °C, the silica chain development illustrated in Fig. 3 ensues from a hetero-condensation of alkoxy groups from TEOS and EETMOS. It is therefore expected that films issued from sols aged at 60 °C are constituted of a continuous silica network in which epoxy groups are homogeneously dispersed, and this

network is all the more developed as TEOS content in sols aged at 60 °C is increased. Differential spectra illustrated in Fig. 3c, d also show that increasing the TEOS content in sols aged at 60 °C does not promote any significant epoxy cycle opening, i.e. no modification of the epoxy band is observed at 885 cm^{-1} in the S20–S0 and S40–S0 differential spectra. These observations mean that, for a fixed duration of aging at 60 °C, a suitable choice of the TEOS content should yield a compromise between sufficient sol reactivity and reasonable stabilization of epoxy groups. A S0 film deposited from a sol aged at 60 °C for 36 h was still partially affected by dewetting defects, though dewetting no longer denuded the substrate contrary to films deposited from non-aged sols. In contrasts, S20 and S40 films deposited from sols aged at 60 °C for 36 h did not suffer any dewetting defect and exhibited good homogeneity and optical quality (see the following section). These observations illustrate that the presence of TEOS in the aged sol is necessary to promote a sufficient reactivity leading to dewetting prevention, in agreement with reactivity features illustrated by IR spectra of Figs. 2 and 3. Partial dewetting was also observed for S40 films deposited from sols aged at 60 °C for 22 h or less, which correlated the reduced reactivity of such sols illustrated by IR spectra of Fig. 2. According to these results, it was finally decided to focus our efforts on an S40 sol aged at 60 °C for 36 h, such conditions being assumed to promote a suitable compromise between an optimal sol reactivity and reasonable stabilization of epoxy groups. Figure 4 shows IR spectra of films deposited from such a sol, which was subsequently aged at room temperature in closed flask for various durations. The initial absence of significant variation in the IR spectra of Fig. 4a, b indicates that the sol remains stable during certain period. This period extended

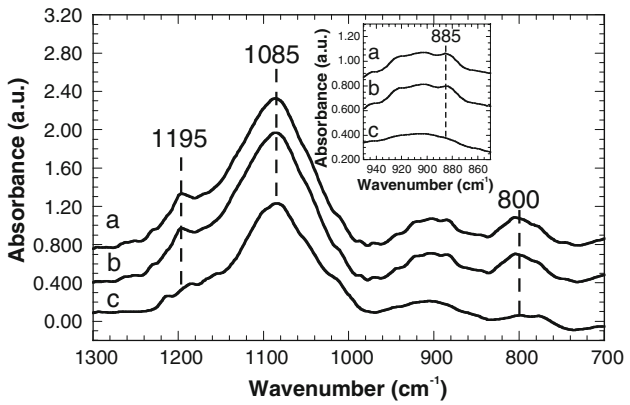

Fig. 4 IR spectra of S40 films deposited from a sol aged at 60 °C for 36 h (a) and from a same sol after subsequent aging at room temperature for 11 days (b) and 18 days (c). Insert shows the same spectra in the epoxy ring spectral region. The EETMOS–TEOS concentration was fixed at 2 M

over 1 week or more, and the stability duration was all the more important as the EETMOS-TEOS concentration in the sol was weak. From these observations, it can be concluded that our sol formulations are compatible with a reasonable in-time reproducibility of films deposited from a same sol. After this initial stability period, sols were observed to evolve with time. The evolution was first appreciated by an increase in the thickness of films deposited from an aged sol, which probably traduced changes in the rheologic properties of the sol (viscosity, surface tension) in relation to its enhanced reactivity. This enhanced reactivity is illustrated in the spectra of Fig. 4b, c. A comparison between these spectra and those illustrated in Fig. 2 shows that, during additional aging at room temperature, the sol undergoes slow chemical changes similar to those rapidly occurring during aging at 60 °C. On the one hand, methoxy groups are more completely consumed and participate to further development of silica chains. On the other hand, insert of Fig. 4 suggests that further consumption of epoxy groups slowly proceeds as well during aging at room temperature. As will be discussed below, the effects of sol aging observed after the initial stability period considerably influenced photopolymerization behaviours of hybrid films. Except when mentioned in the text, in following sections we present results obtained for films deposited from S40 sols aged at 60 °C for 36 h and additionally aged at room temperature for 1 week or less.

Overall film behaviours

Figure 5 illustrates the thickness variations of films deposited from S40 sols of various EETMOS-TEOS concentrations. The films were deposited on 3 × 3 cm^2 silicon wafers with 300 μL of the different sols. The film thickness continuously increases with increasing the precursor concentration. The non-linear variation depicted in this figure probably traduces that increasing the EETMOS–TEOS concentration modifies rheologic properties of the sol (viscosity, surface tension), which in turn influences centrifugal liquid spreading during the spin-coating procedure. As shown in Fig. 5, films up to ca. 5 μm in thickness could be deposited from EETMOS–TEOS sols. Films of 8 μm or more in thicknesses could even be deposited when using greater volumes of sol. All the films exhibited good thickness homogeneity. Ellipsometric measurements performed on ca. 1 and 2 μm thick films deposited on 4 in. Si wafers revealed maximal thickness variations of ±1% through the whole substrate surface. All the films also exhibited a good optical quality, as illustrated in insert of Fig. 5 for 5-μm thick films deposited on glass. Transmission spectra illustrated in this figure indicate maximal diffusion losses of ca. 1% at shorter wavelengths of the

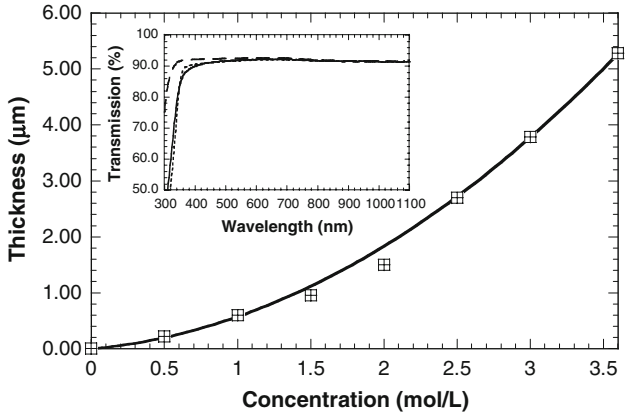

Fig. 5 Influence of the EETMOS–TEOS concentration on the thickness of films deposited from S40 sols aged at 60 °C for 36 h. Insert shows transmission spectra in the UV/visible spectral range for a bare glass substrate (— — —), and for 5 µm thick films deposited on glass, without (- - - - -) or with (——) subsequent exposition to UV lamp for 45 min

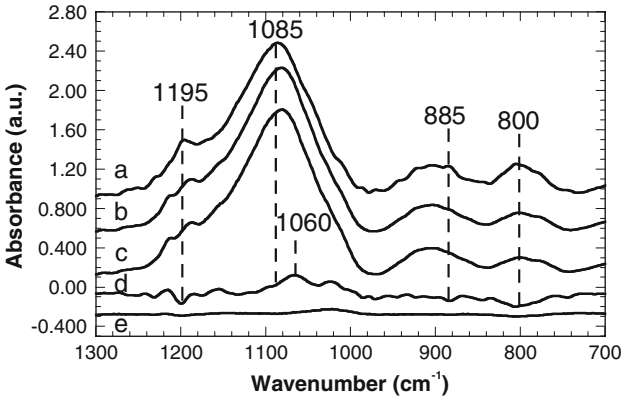

Fig. 6 IR spectra of S40 films deposited from a sol aged at 60 °C for 36 h, before (a) and after UV lamp exposure for 5 min (b) and 40 min (c), as well as 5–0 min (d) and 40–5 min (e) differential spectra for the same films

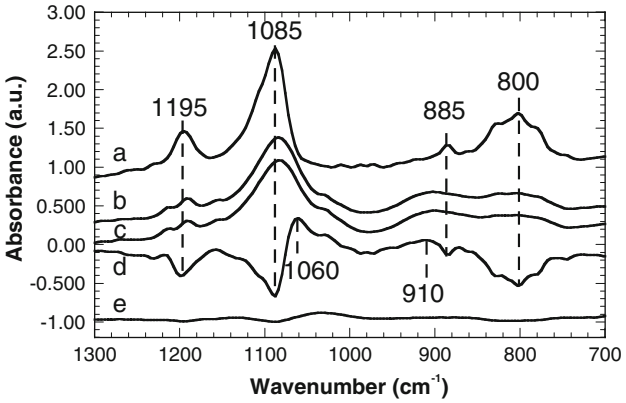

Fig. 7 IR spectra of S0 films deposited from a non-aged sol, before (a) and after UV lamp exposure for 5 min (b) and 40 min (c), as well as 5–0 min (d) and 40–5 min (e) differential spectra for the same films

visible spectrum. This figure also shows that the long-term exposition to UV lamp does not alter the film quality. In these spectra, no typical interference fringes caused by multi-reflexions at film-air and film substrate can be observed. It suggests that the film refractive index is very close to that of the glass substrate, which cancels multi-reflexion mechanisms. This feature was confirmed by ellipsometric measurements. A refractive index of 1.51 ± 0.01 was measured at 633 nm for all films studied in this work, which closely matched the glass substrate refractive index. Absence of interference fringes in transmission spectra also suggests that UV curing does not promote any significant refractive index variation, which will be discussed in the following section. Finally, these spectra show that transmission levels at 365 and 325 nm are around 90 and 60%, respectively. It means that the films rather weakly absorb at the main emission wavelengths of the lamp and laser used for photo-patterning tests, which in turn suggests that even thicker films may be homogeneously photopolymerized in their whole thickness when exposed to UV beam. UV absorption features were confirmed by spectroscopic ellipsometry measurements, showing that maximal values of the film complex index lay in the range 1×10^{-3} at 365 nm to 3×10^{-3} at 325 nm.

Photopolymerization features

Figure 6 shows the IR spectra of films before and after exposition to UV lamp (without mask) for 5 and 40 min. For comparison, same spectra are illustrated in Fig. 7 for films deposited from an S0 sol not aged at 60 °C. IR spectra of Fig. 7 indicate fast chemical modifications occurring during the first 5 min of UV exposure. The (5–0 min) differential spectrum of Fig. 7d shows a negative band at 885 cm^{-1}, which traduces the consumption of epoxy cycles, and two positive bands at 910 and 1,060 cm^{-1}, which indicate the development of polyether chains induced by the photopolymerization of epoxy groups [17, 26]. This differential spectrum also shows the consumption of methoxy groups from EETMOS, which indicates that the photo-induced organic polymerization is accompanied by a sol–gel transformation yielding development of new silica chains. The main IR vibration corresponding to these chains (TO3 mode of silica at 1,080 cm^{-1}) probably contributes to the growth of the 1,060 cm^{-1} band observed in Fig. 7d. The (40–5 min) differential spectrum of Fig. 7e does not show any significant change, which indicates that main photo-induced features take place over the very first minutes of UV exposure. These results confirm the high photo-conversion rate of EETMOS derived films, as already mentioned by Jabbour et al. [24], and also prove

that, despite its weak absorption in the UVA range, our TFP photo-initiator seems to be rather efficient in this spectral range. However, let us recall that films illustrated in Fig. 7 were severely affected by dewetting defects. Compared to Fig. 7, photo-induced features illustrated in Fig. 6 are much less marked. Very small variations can still be appreciated at 800, 885, 1,060 and 1,195 cm^{-1}, which suggests that features illustrated in Fig. 7 also occur in limited extent for films illustrated in Fig. 6. On the one hand, IR band variations illustrated in this figure are very weak because a large part of reactive species (epoxy and methoxy groups) have been consumed upon ageing the S40 sol at 60 °C, as discussed in the previous section. Photo-induced features are thus very close to the sensitivity limits of our IR spectrometer. On the other hand, the differential spectrum of Fig. 6e unambiguously shows that any photo-induced process takes place in the very first minutes of UV exposure, in agreement with data of Fig. 7.

In order to get further insight into photo-induced features, films exposed for various durations to UV lamp (without mask) were characterized by ellipsometry. After UV exposition, the films were rapidly aspersed with ethanol in order to test their stability during the washing procedure involved in photo-patterning tests. Figure 8 illustrates photo-induced thickness variations for films with an initial thickness of ca. 240 nm and 1.5 µm. For the thicker films (Fig. 8a), UV exposure of short duration promotes a slight shrinkage of the thickness, by about 10%, after what further UV curing no longer influences the thickness. This shrinkage probably traduces a photo-induced film densification. No significant refractive index variation could be associated with this densification, in agreement with conclusions drawn from transmission spectra in insert of Fig. 5. It is known that, compared to methacrylate groups, epoxy groups undergo low shrinkage

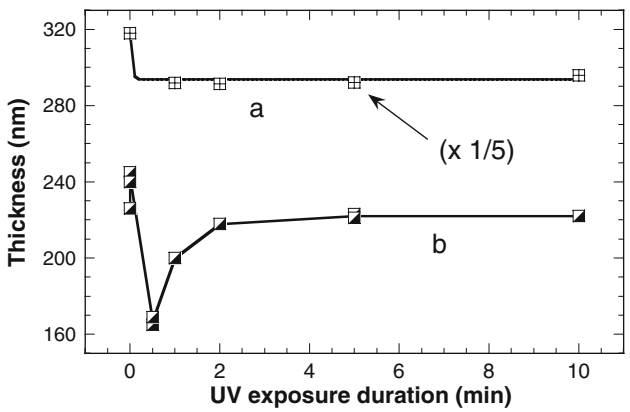

Fig. 8 Photo-induced thickness variations for films with an initial thickness of 1.5 µm (a) and 240 nm (b). UV-cured films were aspersed with ethanol before thickness measurement. Values given for non-cured films have been measured without ethanol aspersion

during photopolymerization [26]. In the case of GPTMS-derived films, Brusatin et al. [23] observed a photo-induced film shrinkage by about 20%, which was associated with a refractive index increase of only +0.01. Since the thickness shrinkage observed in our case is much weaker, it is believed that related refractive index variations are below the accuracy of our experimental conditions (film elaboration and characterization). A similar photo-induced densification is also evidenced in the case of thinner films, yielding film shrinkage by about 10% after UV exposure for 2 min or more (Fig. 8b). However, a shorter UV exposure initially promotes a more pronounced thickness decrease, by about 30 and 15% for films exposed to UV for 0.5 and 1 min, respectively. This feature is due to partial etching of the irradiated film during aspersion with ethanol. This observation indicates that, for films exposed to UV for a too short duration, photopolymerization does not go to completion yielding chemically unstable films. Accordingly, non-irradiated films were fully etched when aspersed with ethanol. As shown in Fig. 8a, the initial thickness reduction caused by etching is not observed for a 1.5-µm thick film exposed to UV for 1 min. It is because, for such exposure duration, etching occurs within a limited depth, of 40 nm or less according to Fig. 8b, which is negligible compared to the 1.5 µm film thickness. In any cases, not only films exposed to UV lamp for 2 min or more resisted to aspersion with ethanol, but they also exhibited rather good mechanical resistance, as shown by rubbing tests with abrasive paper, and good adhesion to substrate, as shown by adhesive tape tests.

Heat-treatments at 80 °C for 10 min were tested on ca. 240-nm thick films in order to assess how low-temperature heat-treatments influence the overall film behaviours. Figure 9 shows the influence of such heat-treatments on the film thickness, in relation to the UV exposure duration. Here again, UV-cured films were washed by rapid aspersion with ethanol. Three heat-treatments were tested, namely a post-deposition heat-treatment performed before UV exposition (Fig. 9b), a post-exposition heat-treatment (Fig. 9c) and a post-washing heat-treatment (Fig. 9d). Films submitted to various heat-treatments are compared with films exempt of any treatment (Fig. 9a). Figure 9 shows that a heat-treatment performed on non-irradiated films promotes a significant thickness reduction, by about 10–15%, compared to non-irradiated films illustrated in Fig. 8. Slight thickness shrinkages can also be appreciated for films heat-treated before UV exposure (see Figs. 8b and 9b). These observations suggest that as-deposited films are in a rather unstable structural state and can undergo partial densification when submitted to a low-temperature heat-treatment. Such a post-deposition densification can also occur in limited extent at room temperature, which would explain certain dispersion in the data of Fig. 9a. However,

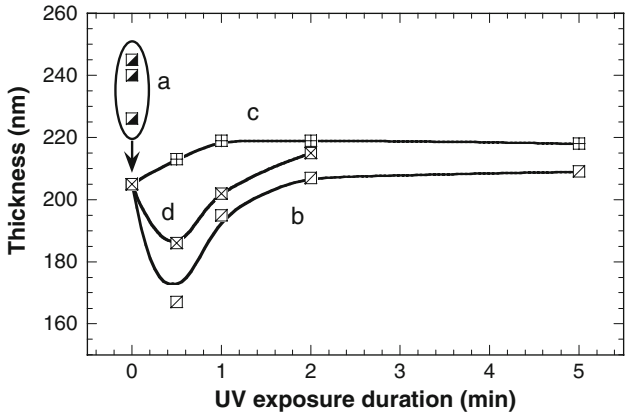

Fig. 9 Effects of heat-treatments at 80 °C for 10 min on the thickness of films exposed to UV lamp for various durations. The films were not heat-treated (a) or heat-treated before UV exposition (b), after UV exposition (c), and after post-exposition ethanol aspersion (d). UV-cured films were aspersed with ethanol before thickness measurement. Values given for non-cured films have been measured without ethanol aspersion

Fig. 9b also indicates that this densification does not prevent partial film etching when washing with ethanol after a short UV exposure of 1 min or less. A comparison between Figs. 8b and 9d shows that a post-washing heat-treatment does not modified the thickness of irradiated films. It suggests that photopolymerization yields a rather stable structural state that inhibits any complementary densification during a subsequent low-temperature heat-treatment. Same conclusions can be drawn from Fig. 9c in the case of films photopolymerized for 2 min or more and subsequently heat-treated before washing. Most salient features are observed in Fig. 9c for films heat-treated after a short UV exposure of 1 min or less, before ethanol aspersion. A film exposed to UV for 1 min exhibits the same thickness as films exposed for longer durations, showing that a post-exposition heat-treatment efficiently prevents subsequent etching by ethanol. Brusatin et al. [21] recently reported that epoxy-based hybrid films deposited from GPTMS could thermopolymerize when heat-treated at around 100 °C, and thermo polymerisation was possible only when heat-treatment was performed on films previously UV cured, provided that the UV dose (product of the light power density by the irradiation time) was insufficient to produce total photopolymerization. Such a complementary thermopolymerization might explain an enhanced chemical stability induced in our film UV-cured for 1 min and subsequently heat-treated at 80 °C, which would promote resistance to ethanol etching. A comparison between films exposed to UV for 0.5 min, as illustrated in Figs. 8b and 9c, also shows that a film heat-treated at 80 °C before ethanol aspersion undergoes a very weak thickness shrinkage compared to a film without heat-treatment. It can signify that the film heat-treated after a 0.5 min UV exposure also undergoes a reduced etching during the final ethanol aspersion. However, since this film is probably not totally photopolymerized after a 0.5 min UV exposure, it can also undergo a partial thermal densification during post-exposition heat-treatment, similarly to what occurs in greater extent for non-cured films. In order to summarize, these results show that, in our experimental conditions, (i) rapid photo-induced features illustrated by IR spectra of Figs. 6 and 7 probably go to completion within 2 min or less, and (ii) a heat-treatment at low temperature performed before ethanol aspersion allows to reduce the UV exposure duration while preventing ethanol etching defects. In following sections, we report on films, deposited from an S40 sol aged at 60 °C for 36 h, and not submitted to any post-deposition heat-treatment.

UV lamp photo-patterning

Preliminary photo-patterning tests were performed through a chromium mask using a UV lamp. Figure 10 shows optical micrographs of 200 nm and 1.5 μm thick films after photo-patterning and ethanol washing. Strips of good homogeneity, corresponding to the negative pattern of the chromium mask, could be imprinted on 200 nm thick films after 0.5 min UV exposure. Figure 10a shows that, in such conditions, a very small strip width of ca. 3 μm can be obtained, which closely corresponds to the weakest inter-motive distance of the chromium mask. However, patterned films were partially etched during ethanol aspersion, in agreement with data of previous section. A very slight increase in strip width is observed in Fig. 10b after 1 min UV patterning and the patterned film was still partially etched by ethanol. Let us recall that, according to previous section, etching effects could be cancelled by a heat-treatment performed before ethanol washing (not tested in this work for patterned films) or by increasing the UV exposure duration. However, Fig. 10c shows that increasing the UV exposure duration, i.e. the UV dose, promotes a dramatic increase in the motive width and partial filling of inter-motive spaces, together with an alteration of the motive edge quality. Finally, a comparison between Fig. 10a and d shows that, for a same short UV exposure duration of 0.5 min, increasing the film thickness also yields a strip width increase: for the narrowest motives, a width of 8 μm is measured for a 1.5-μm thick film compared to 3 μm for a 200-nm thick film. It might be argued that photo-patterning defects illustrated in Fig. 10c, d are due to light refraction effects induced at motive edges of the mask. However, it can hardly be thought that refraction defects propagate on a distance of several microns, as illustrated in Fig. 10c, d. It is thus believed that trends illustrated in this figure are, at least partially, intrinsically influenced by photopolymerization mechanisms.

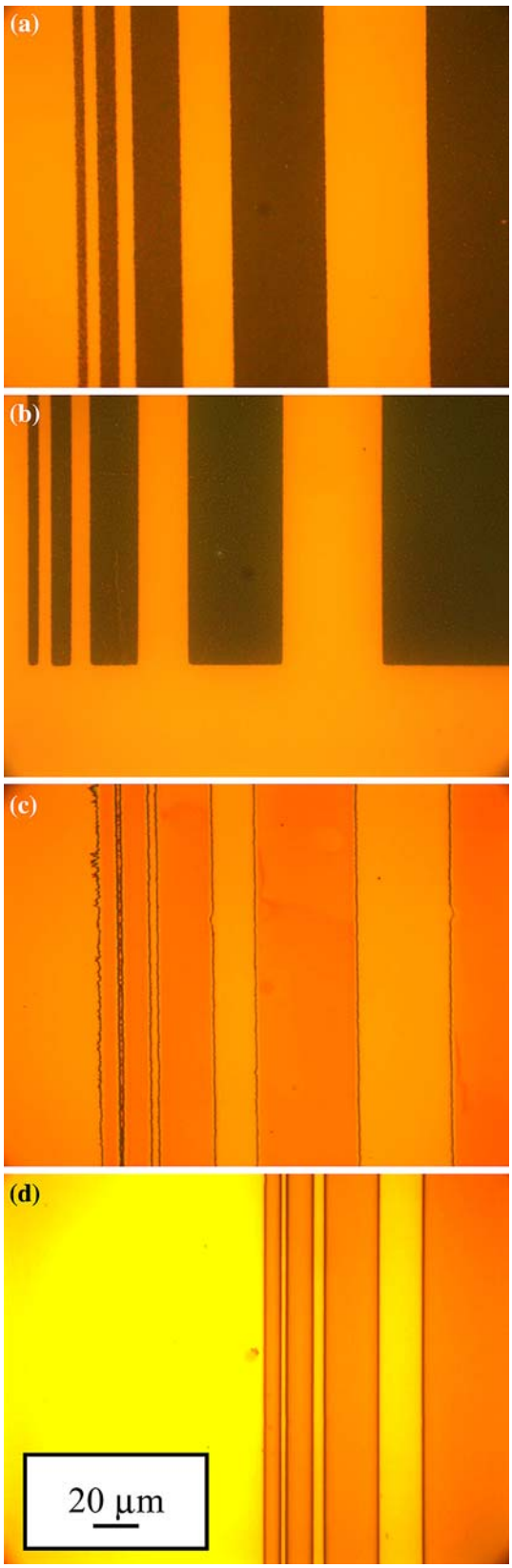

Fig. 10 Optical micrographs of 200-nm thick films photo-patterned through a chromium mask for 0.5 min (**a**), 1 min (**b**), 5 min (**c**), and a 1.5-µm thick film photo-patterned for 0.5 min through the same mask (**d**). Darker areas of the micrographs correspond to the photo-patterned motives. Grey darkness differences observed between micrographs correspond to interference colour effects induced by film thickness differences and/or ethanol etching effects

Croutxé-Barghorn et al. [11] recently reported on the self-generation of relief optical elements in methacrylate-based photosensitive hybrid films, without the need of any post-irradiation wet etching. This self-developing process was based on a mass transfer mechanism involving the flowing of reactive species from non-irradiated areas to irradiated ones, in combination to strain relaxation and surface-free energy effects, which yielded gradual protrusion of a pattern in irradiated areas. In our study, we also observed the self-development of relief in an S40 film deposited from a sol aged at 60 °C for 22 h, submitted to UV exposure through a mask, and not washed with ethanol after UV exposure. This film was partially affected by dewetting defects after deposition, which indicated the rather weak reactivity of the sol in agreement with IR spectra of Fig. 2. Owing to this weak reactivity, development of silica chains in the as-deposited film was probably limited, leading to a silica network of reduced stiffness. This reduced stiffness presumably favoured the segmental mobility of reactive species during UV exposure, which favoured in turn a mass transfer mechanism leading to self-development of relief. Since an S40 sol aged at 60 °C for 36 h is significantly more reactive, it yields a more stiff silica network that probably partially hinders mass transfer. Accordingly, we did not observe any self-development in derived films in the absence of post-irradiation wet etching. However, we cannot exclude that such a mass transfer occurs in limited extent, which might alter the photo-patterning process and participate in progressive motive width increase and inter-motive space filling, as illustrated in Fig. 10. Croutxé-Barghorn et al. [11] also pointed out that polymerization could pursue for certain time in dark condition through additional development of organic chain initially formed in irradiated areas, which in turn participated in relief formation mechanisms. It is known that polymerization of epoxy species can also pursue for certain time after UV light switching off [17]. It particularly suggests that organic polymeric chains can also propagate from irradiated areas towards non-irradiated ones during exposition through a mask, and this propagation should be all the more pronounced as UV exposure is prolonged. A possible propagation of polymeric chains, occurring during UV exposure from irradiated to non-irradiated areas, should reinforce the chemical stability in non-irradiated areas, which would present in turn enhanced resistance to ethanol washing. This second mechanism can thus participate as well in motive width increase and inter-motive space filling occurring upon UV irradiation. Figure 10d also indicates that photo-patterned motive degradation occurs more

rapidly in thicker films. During the post-deposition sol–gel transformation, the formation of a solid xerogel films takes place through the development of silica chains and densification of the so-formed silica network promoted by capillary forces induced by solvent evaporation. A dense and stiff silica network rapidly forms at the external surface, which hinders in turn reactions in deeper layers of the film. Hindering in deeper layer should be all the more marked as films are thicker. It means that deeper layers of a thicker film are constituted of a less stiff silica network than in thinner films. Accordingly, during our photo-patterning tests through chromium mask, we have observed that films of thickness >1.5 μm partially stick to the mask, which confirms that thick films are globally less reacted than thinner ones. A less stiff silica network formed in thicker films can then favour a greater mobility of reactive species during UV exposure through the mask, which may in turn explain features illustrated in Fig. 10d on the basis of mater transfer mechanisms and/or propagation of polymeric chains into non-irradiated areas.

Figure 11 illustrates FEG-SEM and AFM analyses of a 1.5-μm thick film photo-patterned through chromium mask for 0.5 min and subsequently washed with ethanol. The cross-sectional FEG-SEM image illustrated in Fig. 11a shows rather homogeneous linear strips and confirms a width of ca. 8 μm for the narrowest strips, in agreement with the data of Fig. 10d. However, this image also shows that strip edges are not vertical. Slopes at strip edges were analysed by AFM. This analysis confirmed the homogeneity of the patterns and presence of a slope at the edges. Figure 11b shows the pattern profile for a same sample area as that illustrated in Fig. 11a. A slope of ca. 35° can be appreciated. It should be noticed that slope artefacts can ensue from the conical shape of the tip used for AFM measurements. However, a simple calculation accounting for the aperture angle of our AFM tip (70°) shows that slopes <55° cannot be induced by tip effects. Figure 11b also shows that the strip profiles are slightly rounded at their top and the pattern thickness is slightly greater than that of the initial film, i.e. about 1.8 vs. 1.5 μm. Slope and rounded shape effects obviously introduce an error in the strip widths estimated from optical micrographs of Fig. 10. Widths estimated from optical micrographs are probably underestimated and more presumably correspond to widths at top of the strips. It is believed that appearance of a slope at strip edges might depict preliminary states of mechanisms progressively leading to inter-motive spaces filling, as illustrated in Fig. 10, and the increased thickness and weakly rounded shape illustrated in Fig. 11b might as well traduce slight self-developing effects as discussed above. Though these preliminary results obviously require improvements, they demonstrate the feasibility of photo-patterning our EETMOS–TEOS films and they confirm that rapid photopolymerization features discussed in previous section lead to a fast photo-patterning, which allows reducing the necessary UV dose. However, let us recall that films studied in this section were deposited from an S40 sol, aged at 60 °C and subsequently aged at room temperature for 1 week or less. Some punctual tests showed that, when films were deposited from a sol additionally aged at room temperature for a longer duration, photo-patterning efficiency was considerably reduced. In that case, films exposed through a mask for 2 min or less were totally etched after aspersion with ethanol, and a UV exposure duration of 5 min was necessary to reproduced features obtained after only 0.5 min exposure when films were deposited from a sol aged at room temperature for a short duration. These observations have to be related to the data of Fig. 4 showing that, after an initial stability period, sols aged at room temperature undergo significant chemical modifications. On the one hand, an enhanced sol–gel reactivity of aged sols yields further development of silica chains in the film, which probably enhance the stiffness of the resulting silica network. The mobility of reactive species should thus be reduced, which may hinder organic photopolymerization mechanisms. On the other hand, a possible complementary opening of epoxy rings in the aged sol should decrease the amount of reactive species in the film, which would also contribute to reduce the photopolymerization efficiency.

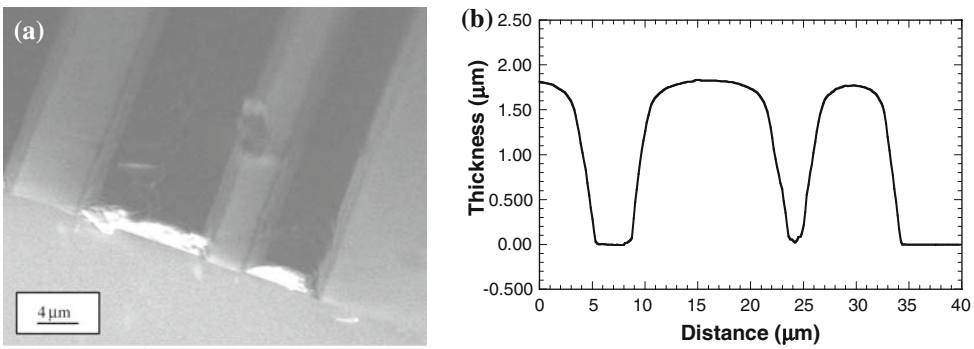

Fig. 11 Cross-sectional FEG-SEM image of a ca. 1.5-μm thick film photo-patterned for 0.5 min through a chromium mask (**a**) and AFM analysis of pattern profiles for the same sample (**b**)

Laser photo-patterning

Previous results have shown that, despite some ethanol etching problems essentially observed for the thinnest films, reducing the UV dose leads to the best results in terms of photo-pattern quality. As illustrated in previous section, when using a lamp and mask system, varying the exposure duration is the easiest way to control the UV dose. In contrast, a laser system allows a much more flexible control of the UV dose through the variation of multiple parameters, including the laser power or imprinting speed. In this paper, we have chosen to fix a constant light power of 30 mW and to study the quality of laser imprinted patterns with respect to the imprinting speed and laser lens position. Results are illustrated in Fig. 12 for 2.3-μm thick films. It appears that imprinting speed and lens position markedly influence the width of patterned strips, as determined from optical microscope observations. A minimal width of 4–5 μm can be obtained in optimized focalization conditions when using a rapid imprinting speed of 5 mm/s (Fig. 12a). This width nearly corresponds to the laser spot diameter (4 μm). It means that, in the experimental conditions tested here, narrower widths can hardly be envisaged. Accordingly, a 200-nm thick film patterned in similar laser exposure conditions did not exhibit narrower strip widths (not illustrated here). Figure 12a shows that, for a 5 mm/s speed, the strip width also lies in a 4–5 μm range when varying the lens position between 0 and 40 μm (to be compared to the 2.3 μm film thickness), which expresses that laser beam focalization is not a very critical parameter. In contrast, when varying the lens position in a wider range of values, de-focalization promotes considerable losses of resolution, yielding strip widths up to 10 μm or more. In optimized focalization conditions, minimal strip widths of 4–5 μm were also measured for imprinting speeds ranging between 5 and 2 mm/s. This result indicates that, in this range of values, imprinting speed does not play a critical role in the laser patterning process. However, decreasing the imprinting speed also promoted a more critical influence of the lens position on the strip width. These features are illustrated in Fig. 12b for a speed of 2 mm/s. Further speed decrease, i.e. UV dose increase, yielded a more pronounced increase in the strip width, leading to a minimal value of ca. 8 μm for a 0.5 mm/s speed (Fig. 12c). These latter results indicate that influence of the imprinting speed nearly correlates that of the UV exposure duration illustrated in Fig. 10a, c in the case of a mask photo-patterning, which confirms previously drawn conclusions on the effects of UV dose. Effects of imprinting speed and lens position similar to those illustrated in Fig. 12 were also observed in the case of thicker films (not illustrated here). In particular, a rapid imprinting speed and optimized focalization conditions yielded a minimal strip width comparable to that deduced for thinner films (see below). This observation shows that thickness effects illustrated in Fig. 10a, d for a mask and lamp procedure are suppressed or considerably reduced when films are photo-patterned with a laser beam. It depicts that a laser technique provides a more accurate and flexible control of UV dose, which authorizes the patterning of thicker films without noticeable resolution losses.

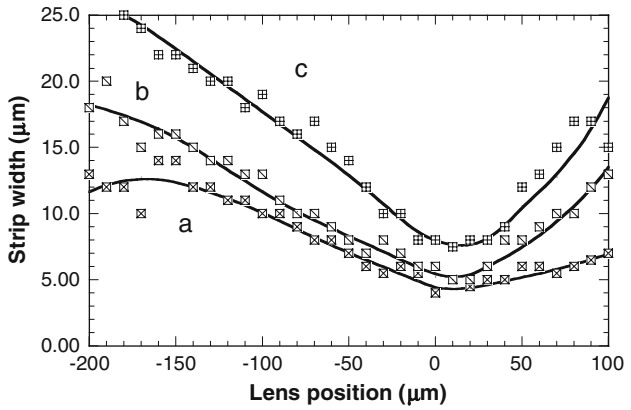

Fig. 12 Influence of the laser lens position on the width of strips imprinted on a 2.3-μm thick film with imprinting speeds of 5 mm/s (a), 2 mm/s (b), and 0.5 mm/s. The laser power was fixed at 30 mW. Lines are drawn to guide the eyes

Figure 13 shows strip profiles deduced from AFM analyses for 2.3 and ca. 8-μm thick films laser patterned in optimized focalization conditions with an imprinting speed of 5 mm/s. For the 2.3-μm thick film (Fig. 13a), the strip profile exhibits a flat surface with rounded corners. As mentioned before, these rounded corners probably introduce a certain underestimation of strip widths determined from optical observations, as illustrated in Fig. 12. The strip thickness of 2.3 μm, as also confirmed by profilometry measurement, exactly matches that of the as-deposited (non-patterned) film, which indicates that weak possible effects of photo-densification and post-irradiation ethanol etching may be compensated for by a slight thickness increase, according to mechanisms discussed before for a mask patterning procedure. However, this increasing thickness effects appear to be very weak compared to those involved for the film illustrated in Fig. 11b. It means that, using a laser patterning procedure, previously discussed possible mater transfer and polymeric chain propagation mechanisms should proceed in very limited extent compared to a mask procedure. For the profile illustrated in Fig. 13b, a strip thickness of ca. 8 μm was determined by profilometry. For such a thickness, only the upper part of the strip could be accurately probed by the AFM tip, owing to limitations due to the tip height (ca. 3 μm) that introduced intrinsic measurement artefacts when too thick profiles were analysed (see arrow in Fig. 13b). Upper part

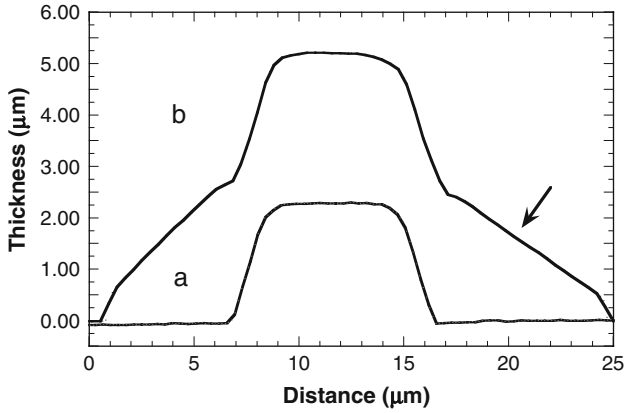

Fig. 13 AFM analysis of strip profiles obtained by laser patterning a 2.3 µm (a) and a ca. 8-µm thick film (b) in optimized focalization conditions with an imprinting speed of 5 mm/s. Slopes observed in the lower part of the thicker profile (see arrow) are due to AFM tip artefacts, as discussed in the text

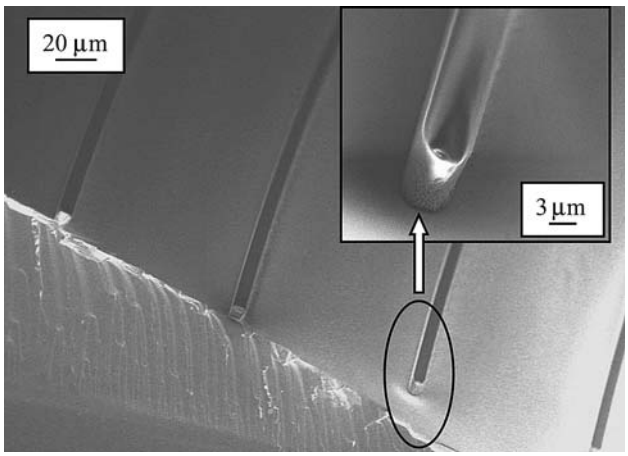

Fig. 14 FEG-SEM images of strip profiles obtained by laser patterning a ca. 8-µm thick film in optimized focalization conditions with an imprinting speed of 5 mm/s

of this strip exhibits shape and width rather similar to those of the 2.3-µm thick strip (except a slightly more rounded surface). It confirms that photo-induced thickness effects, illustrated in Fig. 10a, d in the case of a mask and lamp procedure, occur in very limited extent for laser-patterned films. Figure 13 also shows that strips of different thickness exhibit similar slopes at their edges. However, these slopes are extremely close to the threshold value of 55°, where the cone-shaped AFM tip introduces measurements artefacts, as discussed before. Figure 14 shows FEG-SEM images of strips laser patterned in optimized focalization conditions with an imprinting speed of 5 mm/s. Slightly rounded corners at top of the strips are confirmed, but these images unambiguously demonstrate that slopes illustrated in Fig. 13 are due to AFM measurement artefacts and that laser patterned strips exhibit rather vertical edges. Vertical edges were also confirmed by FEG-SEM characterization of laser patterned 2.3 µm thick films. These new observations confirm that, in our experimental conditions, (i) a laser patterning procedure yields much better photo-patterned profiles than a mask and lamp procedure, and (ii) our EETMOS-based films are adapted to the patterning of very good quality motives using a UVA laser-patterning technique. It is concluded that, besides intrinsic performances of an EETMOS-based hybrid system, the laser-patterning procedure used in this work provides two main assets compared to a masking method. On the one hand, due to a rapid imprinting speed, the irradiation duration per surface unit is considerably weaker in the case of laser-patterned films compared to that involved in the case of films discussed in previous section, which may drastically reduce the extent of previously discussed parasitic mechanisms yielding width increase and deformation of the photo-patterned motives. On the other hand, the ca. 10 µm field depth provided by our laser patterning device, which yields a constant photonic energy through a long optical path of constant section, permits a rather large de-focalization tolerance, while allowing homogeneous photopolymerization through the thickness of rather thick films, which guarantees similar qualities of profiles laser patterned in films of very different thicknesses. According to these first promising results, further works will be devoted to laser patterning of more complex shape motives and/or reduced size motives using a 1-µm diameter laser spot.

Conclusion

Photosensitive EETMOS-based sol–gel hybrid films have been studied. EETMOS sols have been optimized in order to fulfil several criteria: (i) sufficient sol reactivity that prevents detrimental film dewetting defects, (ii) controlled sol reactivity that guarantees stability compatible with the in-time reproducible deposition of hybrid films using a same sol and (iii) sufficient stabilization of photo-sensitive species in the sol that preserves good photosensitivity of derived hybrid films. Hybrid films, deposited by spin-coating from optimized sols, exhibit good optical quality and thickness homogeneity. Photo-sensitivity of EETMOS-based hybrid films has been assessed by UVA exposure experiments. FTIR and ellipsometry characterizations depict fast photo-induced mechanisms induced by an efficient cationic photopolymerization mechanism. Functionality of these films has been assessed through photo-patterning tests using a mercury lamp or a He–Cd laser source emitting in the UVA spectral range. Both sources yield micronic-sized patterns, which demonstrates the good sensitivity of an optimized EETMOS system to UVA light. These tests evidence effects of the UV dose on the quality of derived patterns. Superior

quality of laser-patterned motives is demonstrated, which is attributed to a more accurate and flexible control of UV dose using a laser technique. Further works will be devoted to laser patterning of complex shape and/or reduced size motives.

References

1. Dunn B, Mackenzie JD, Zink JI, Stafsudd OM (1990) SPIE Proc 1328:174. doi:10.1117/12.22557
2. Schmidt H, Krug H, Kasemann R, Tiefensee F (1991) SPIE Proc 1590:36. doi:10.1117/12.50199
3. Krug H, Schmidt H (1994) N J Chem 18(10):1125
4. Coudray P, Chisham J, Malek-Tabrizi A, Li CY, Andrews MP, Peyghambarian N et al (1996) Opt Commun 128:19. doi:10.1016/0030-4018(96)00101-0
5. Ou DL, Adamjee A, Lana SL, Seddon AB (1996) Surf Coat Int 11:496
6. Coudray P, Chisham J, Andrews MP, Najafi SI (1997) Opt Eng 36(4):1234. doi:10.1117/1.601243
7. Etienne P, Coudray P, Moreau Y, Porque J (1998) J Sol–Gel Sci Tech 13:523
8. Innocenzi P, Martucci A, Guglielmi M, Armelao L, Pelli S, Righini GC et al (1999) J Non-Cryst Sol 259:182
9. Park OH, Jung JI, Bae BS (2001) J Mater Res 16(17):2143. doi:10.1557/JMR.2001.0292
10. Soppera O, Croutxé-Barghorn C, Lougnot DJ (2001) N J Chem 25:1006. doi:10.1039/b102317a
11. Croutxé-Barghorn C, Soppera O, Chevalier M (2003) Macromol Mater Eng 288:219. doi:10.1002/mame.200390020
12. Saravanamuttu K, Blanford CF, Sharp DN, Dedman ER, Turberfield AJ, Denning RG (2003) Chem Mater 15:2301. doi:10.1021/cm034015i
13. Trejo-Valdez M, Jenouvrier P, Fick J, Langlet M (2004) J Mater Sci 39:2801. doi:10.1023/B:JMSC.0000021457.85382.1c
14. Zhang X, Lu H, Soutar AM, Zeng X (2004) J Mater Chem 14:357. doi:10.1039/b310309a
15. Soppera O, Moreira PJ, Leite AP, Marques PVS (2005) J Sol–Gel Sci Tech 35:27
16. Decker C (1998) Polym Int 45:133. doi :10.1002/(SICI)1097-0126(199802)45:2<133::AID-PI969>3.0.CO;2-F
17. Decker C, Nguyen Thi Viet T, Le Xuan H (1996) Eur Polym J 32:1319. doi:10.1016/S0014-3057(96)00058-4
18. Rajaraman SK, Mowers WA, Crivello JV (1999) J Polym Sci Part Polym Chem 37:4007. doi :10.1002/(SICI)1099-0518(19991101)37:21<4007::AID-POLA15>3.0.CO;2-8
19. Crivello JV (2002) Radiat Phys Chem 63:21. doi:10.1016/S0969-806X(01)00476-5
20. Cheng X, Jay Guo L, Fu PF (2005) Adv Mater 17:1419. doi:10.1002/adma.200401192
21. Brusatin G, Della Giustina G, Guglielmi M, Innocenzi P (2006) Prog Solid State Chem 34:223. doi:10.1016/j.progsolidstchem.2005.11.005
22. Brusatin G, Della Giustina G, Romanoto F, Guglielmi M (2008) Nanotechnique 19:1. doi:10.1088/0957-4484/19/17/175306
23. Brusatin G, Della Giustina G, Guglielmi M, Casabolni M, Prosposito P, Schutzmann S et al (2007) Mater Sci Eng C 27:1022. doi:10.1016/j.msec.2006.06.020
24. Jabbour J, Callas-Etienne S, Smaihi M, Gatti S, Kribich R, Pille G et al (2007) Appl Surf Sci 253:8032. doi:10.1016/j.apsusc.2007.02.079
25. Jabbour J, Callas S, Smaihi M, Gatti S, Etienne P (2008) J Non-Cryst Sol 354:1001
26. Jabbour J, Callas S, Gatti S, Kribich R, Myara M, Pille G et al (2008) J Non-Cryst Sol 354:651
27. Capozzi CA, Pye LD (1988) Proc SPIE 970:135
28. Babonneau F, Maquet J (2000) Polyhedron 19:315. doi:10.1016/S0277-5387(99)00361-7
29. Viart N, Rehspringer JL (1996) J Non-Cryst Sol 195:223
30. Philipp G, Schmidt H (1986) J Non-Cryst Sol 82:31
31. Nass R, Arpac E, Glaubitt W, Schmidt H (1990) J Non-Cryst Sol 121:370
32. Schmidt H, Seiferling B (1986) Mater Res Soc Symp Proc 73:739
33. Primeau N, Vautey C, Langlet M (1997) Thin Solid Films 310:47. doi:10.1016/S0040-6090(97)00340-4